Raman *G* band in double-wall carbon nanotubes combining *p* doping and high pressure

Pascal Puech,[1,*] Ahmad Ghandour,[2] Andrei Sapelkin,[2] Cyril Tinguely,[3] Emmanuel Flahaut,[3] David J. Dunstan,[2] and Wolfgang Bacsa[1]

[1]*Cemes, Université Paul Sabatier, 29 rue Jeanne Marvig, 31055 Toulouse, France*

[2]*Department of Physics, Queen Mary, University of London, London E1 4NS, United Kingdom*

[3]*CIRIMAT-LCMIE, UMR CNRS 5085, Université Paul Sabatier, 118 Route de Narbonne, 31062 Toulouse, France*

(Received 22 January 2008; published 10 July 2008)

We use sulfuric acid as pressure medium to extrapolate the *G*-band position of the inner and outer tubes of double-wall carbon nanotubes. Keeping the *G*-band position of the inner and outer tubes constant, we can determine the fraction of double-wall and single-wall tubes in samples containing a mixture of the two. *A*-band-related electronic interwall interaction at 1560 cm^{-1} is observed, which is associated with the outer tube walls. This band is observed to shift with pressure at the same rate as the *G* band of outer tubes and is not suppressed with chemical doping. Differences in the interwall interaction is discussed for double-wall carbon nanotubes grown by the catalytic chemical-vapor method and double-wall carbon nanotubes obtained through transformation of peapods.

DOI: 10.1103/PhysRevB.78.045413 PACS number(s): 63.22.−m, 62.25.−g, 81.07.De

I. INTRODUCTION

Double-wall carbon nanotubes (DWs) are the simplest form of multiwall carbon nanotubes, while single-wall carbon nanotubes (SWs) can be either semiconducting or metallic, depending on the orientation of the graphene sheet with respect to the tube axis. Multiwall carbon nanotubes (MWs) are metallic. The electrical conductivity of graphene is highly anisotropic. Perpendicular to the graphene layer, the conductivity of σ bonds is less than 1% of the in-plane electrical conductivity.[1] The electronic conductivity in MWs has been extensively studied, and the observed intershell conductance is consistent with tunneling through orbitals of neighboring walls.[2] DWs are suitable for the study of interwall coupling.

Two main synthesis methods for DWs are known today: conversion of peapods leading to DWs with a narrow diameter distribution,[3] and the use of the catalytic chemical-vapor deposition (CCVD) method resulting in 80%–100% of DWs with a broader diameter distribution.[4,5] Raman spectroscopy is routinely used to screen the carbon nanotubes (CNTs). The diameter distribution can be obtained from the low-frequency radial breathing mode as a function of excitation wavelength and the quality can be assessed by measuring defect-induced scattering (*D* band).[6]

The *G* band in DWs contains contributions from the internal and external tubes, which depend on external parameters such as pressure, temperature, and applied electric field.[7] The *G* bands of the inner and outer tubes do not fall on the same spectral position since the pressures experienced by the inner and outer tubes are different.

We combine the influence of the *G*-band shape as a function of chemical doping and hydrostatic pressure to separate contributions from inner and outer tubes and to assign an additional spectral band at the lower-energy side of the *G* band. Internal tubes in DWs are subject only to the pressure from the outer tube and are less affected by doping (10%).[8] We therefore use the contributions of the internal tubes as a reference.[9] The DWs are not open in general and contain no larger wall defects.[10] Filling of DWs would also imply changes in the *G*-band position of the internal tubes under hydrostatic pressure, which we have not observed. We therefore assume that the DWs are not filled, which is consistent with what is observed using high-resolution electron microscopy.

The spectral *G*-band position of the outer tube in DWs falls at the same frequency range of the G_+ band in SWs, which makes it impossible to separate different *G*-band contributions. Kim *et al.*[11] recently proposed a scheme to determine the purity in DW samples which contain DWs and SWs using chemical doping. Chemical doping with sulfuric acid has a large effect on the *G* band of SWs (Ref. 12) and DWs.

We find that Raman spectra of DWs doped with H_2SO_4 as reported in literature[11,13] are interpreted differently. We use hydrostatic pressure–induced spectral changes to separate the different spectral contributions to the Raman *G* band and to clarify the interpretation of doping-induced spectral changes.

Hydrostatic pressure has been used to separate the contributions of the inner and outer tubes to the *G* band.[14,15] The *G*-band position of the inner tube when applying pressure is found to be close to the *G* band observed for graphite, while for the outer tube the *G* band shifts to higher frequency with increasing pressure. We combine chemical doping with hydrostatic pressure using sulfuric acid as pressure transmitting medium to find the experimental parameters to determine the fraction of DWs and SWs in DW samples. The differences observed between the two types of DW samples presents us with the possibility of exploring interwall interaction in double-wall carbon nanotubes. We apply the extracted and experimentally deduced parameters in fitting the *G* band when heating DWs in air.

II. SAMPLE AND EXPERIMENTS

We have used DWs prepared by the CCVD method[16] and for comparison, we have used SWs with 0.8 nm diameter (HiPco) and SWs with 1.4 nm diameter (NanoCarbLab). High-resolution transmission electron microscopy (HRTEM)

 ©2008 The American Physical Society

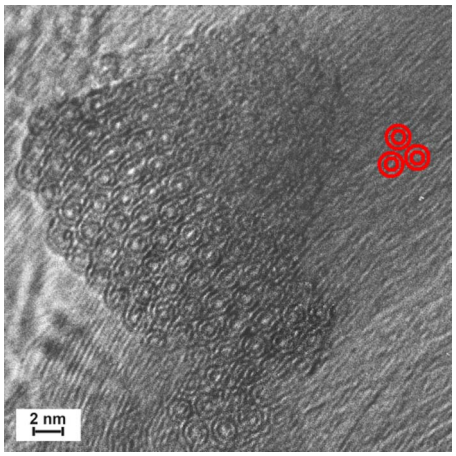

FIG. 1. (Color online) Transmission electron microscopy images of DWs.

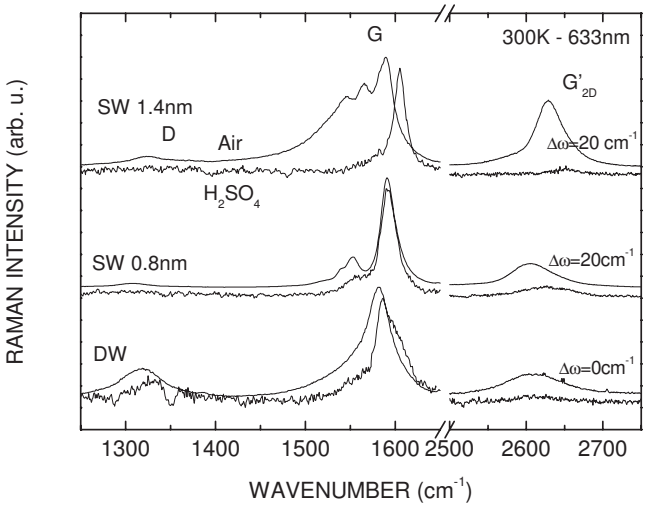

FIG. 2. Effect of doping with H_2SO_4 on Raman spectra of SW and DWs excited at 633 nm.

images show the presence of individual and small bundles of DWs with diameters ranging from 0.6 to 3 nm (see Fig. 1). In the CCVD method individual CNTs are grown from catalytic particles formed *in situ* through selective reduction of cobalt oxide to cobalt nanoparticles. After the chemical etching of the catalyst, the tubes agglomerate into bundles through van der Waals interaction. Frequent formation of interstitial channels is expected due to the broad diameter distribution (2–3 nm). The diameter has been measured in HR-TEM images of a hundred isolated CNTs to obtain a diameter distribution.[16] The tubes are found to be single ($\approx$15%), double (80%), or triple walled ($<$5%). A typical transmission electron microscope image is shown in Fig. 1.

We use a Renishaw Raman microprobe instrument to record spectra for the high-pressure experiment at room temperature. A microscope objective ($\times$20) was used to focus the laser beam (633 nm) on the sample inside the pressure anvil cell. The laser output power was kept low to avoid heating. Heating effects are relatively less important at 633 nm than at shorter wavelengths.[17] In general we have used laser powers at least four times smaller than what is needed to cause heat-induced spectral changes.

The high-pressure Raman measurements were performed in a diamond anvil cell. The pressure was monitored using the luminescence of a ruby chip inside the cell and the DWs were dispersed in sulfuric acid by sonication.

For the 647 nm excitation wavelength, the Raman spectra were recorded using a XY-Dilor spectrometer. The beam power had been measured at the laser. To compare laser power values accurately, one needs to take into account the Gaussian beam profile, the transmission factor of the microscope (1/10 for visible XY-Dilor system), tube orientation, tube bundling, and surrounding medium (gas, liquid, or substrate).

III. USING H_2SO_4 AS PRESSURE MEDIUM

A. *p*-doping effect at atmospheric pressure

Zhou *et al.*[12] showed that the spectral *G*-band position of SWs depends on the diameter and the exciting wavelength when doping. The spectral shift is attributed to doping-induced strain and charge transfer, which can be estimated with corresponding shifts in graphite intercalation compounds.[18]

The *G* band shifts by 16 cm^{-1} for the first H_2SO_4 intercalation stage and shifts two or three times this value for the second and third intercalation stages.[19] High-pressure experiments[20] on intercalated graphite show that the lattice parameter $\delta a/a$ changes by 8×10^4 for each stage, resulting in a strain-induced shift of 4 cm^{-1}. The remaining shift of 12 cm^{-1} can be attributed to modification of the electron-phonon interaction due to charge transfer.[21] Consequently, doping-induced shifts in DWs can be attributed to changes in the electron-phonon coupling after subtracting strain-induced shifts as observed for intercalated graphite.

In Fig. 2, we show Raman spectra excited at 633 nm in the spectral region of the *D* and *G* bands and the G'_{2D} band of SWs (diameters: 1.4 and 0.8 nm) and DWs. All spectra have been recorded in air form samples before and after doping using 1 mW.

We note that SWs with an average diameter of 1.4 nm show a doping-induced shift of the *G* band to higher frequencies. Contributions from the G_- band in SWs are strongly reduced in intensity or absent when doped for 1.4 nm diameter SWs. The average tube diameter in DWs and SWs are larger than 1.4 nm in our DW sample and we expect a large upshift as a result of chemical doping. However, we observe a narrower *G* band after doping for DWs containing $\approx$15% of SWs and no upshift. To understand this difference, we examine in Sec. III B the influence of hydrostatic pressure on the *G* band of doped DWs.

B. Hydrostatic pressure

At normal pressure, i.e., without anvil cell, the *G* band shows no apparent contributions from the inner and outer tubes. When applying pressure, as seen in Fig. 3, the *G* band from the outer tube shifts to higher frequencies at a larger rate and the intensity of the *G* band of the inner and outer

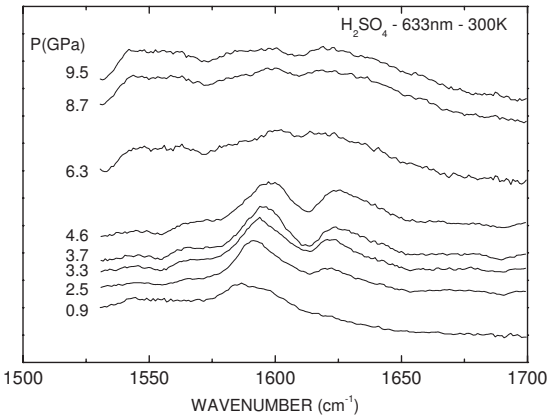

FIG. 3. *G* band of DW sample for pressures up to 9.5 GPa using H_2SO_4 as pressure transmitting medium.

tubes is comparable at high pressure (>4 GPa). The contribution to the *G* band from SWs in the DW sample is also present but is less intense and not spectrally resolved at high pressure. At around 5 GPa we observe a decrease in the intensity of all the contributions to the *G* band, which we attribute to a possible freezing of the medium.

In Fig. 4, we have plotted the spectral position of the *G* band corresponding to the inner and outer tubes and the relative intensity of the two main bands as a function of hydrostatic pressure. We can clearly notice the pressure-induced transition at 5–6 GPa when the spectral shift and the intensity saturates.

The relative small pressure-induced spectra shifts for both inner and outer tubes (see Table I) using H_2SO_4 as pressure medium is explained by the formation of ordered molecular shells on the surface of the tubes, which has the effect of reducing the pressure experienced by the tubes.[9,22] Figure 4 shows how the *G* band of the outer tubes increases significantly in intensity with increasing pressure when compared to the *G* band of the inner tubes. From the *G*-band shift with pressure, we extrapolate the *G*-band position at zero pressure. Interestingly, the intensity associated with the outer tube is vanishingly small at zero pressure when excited at

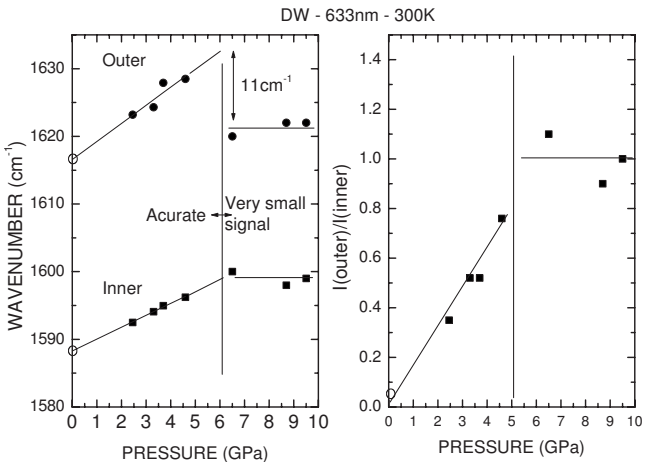

FIG. 4. *G*-band position of inner and outer tubes in function of pressure (left) and intensity ratio (right).

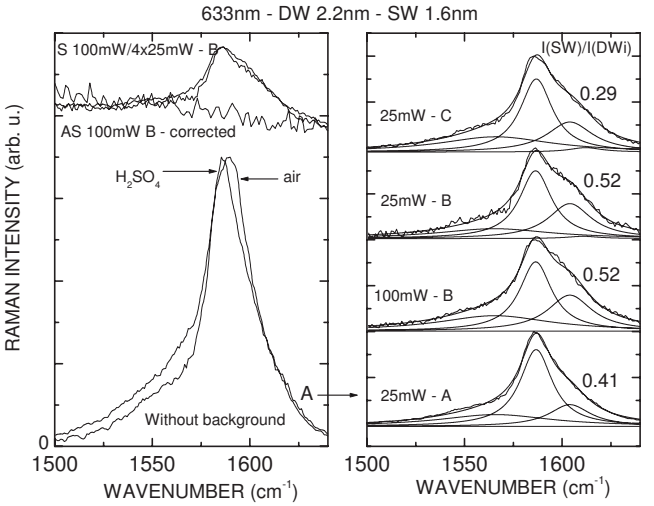

FIG. 5. Doped and undoped Raman spectra of *G* band of DW sample on three different locations (A, B, and C): Stokes (S) and anti-Stokes (AS) spectra after including the Bose-Einstein (T =775 K) and ω^4 factors.

633 nm. It is expected that doping moves the Fermi level into the valence band, which changes the resonant transition energies of the outer tubes.

C. Deducing the purity of DW samples

To determine the fraction of DWs and SWs in the sample, we use the spectral *G*-band position extrapolated in Fig. 4. Figure 5 shows the *G*-band spectra of DW samples recorded at three different locations (A, B, and C) and recorded at different laser power levels. The left-hand side shows Stokes and anti-Stokes spectra at location B and a spectrum of DWs in H_2SO_4. To match the background level for Stokes and anti-Stokes spectra, we have corrected the anti-Stokes part by ω^4 and included the Bose-Einstein factor using T =775 K. This high temperature is attributed to single-particle excitations.[23] We note that no significant *G* band is recorded for the Stokes spectrum. On the right side of Fig. 5, we have subtracted a linear background for each spectrum for the three locations A, B, and C.

To fit the *G* band, we take into account four spectral contributions: the spectral positions for inner and outer tubes of DWs as extrapolated from high-pressure experiments, the G_+ band of SWs, and an electronic coupling interwall (EI)–induced band located at 1568 cm^{-1}. We keep the spectral positions constant and take the intensities of the four contributions as free parameters. The fitting parameters, as deduced from the hydrostatic experiment, are reported in Table II. We find that even if a small spectral shift is allowed for the four bands, the intensity ratio remains unchanged. For location B, we show the spectra for two different laser powers. The fit remains stable and the higher power has the effects of simply reducing the spectral noise.

From the result of the fit, we can take the ratio of the intensity of the two *G*-band contributions corresponding to SWs and the inner tubes of DWs. We assume that the ratio of the number of SW tubes and DW tubes, N_{SW}/N_{DWi}, is pro-

TABLE I. Spectral *G*-band positions of inner and outer tubes of DWs, corresponding pressure coefficients, relative intensities, and spectral positions of the shoulder for four different pressure transmitting media (excitation wavelength, 633 nm) (*i*: inner tube; *o*, outer tube; EI, electronic interwall).

Medium	$\omega_i(P=0)$ (cm^{-1})	$\omega_o(P=0)$ (cm^{-1})	$d\omega_i/dP$ (cm^{-1} GPa^{-1})	$d\omega_o/dP$ (cm^{-1} GPa^{-1})	$d\omega_i/d\omega_o$	$I(i)/I(o)$	$\Gamma_{i\text{-}o}(P=0)$ (cm^{-1})	$\omega_{EI}(P=0)$ (cm^{-1})	Γ_{EI} (cm^{-1})
Me-Et	1582	1594	3.3	5.8	0.57	1.04	9	1560	35
O_2	1584	1598	4.1	6.9	0.59	0.64	10	1560	35
Argon	1581	1592	5.1	8.6	0.59	0.54	13	1560	35
H_2SO_4	1587	1618	2.2	$\approx 2.1(\pm 30\%)$		Linear	10		

portional to the ratio of intensities of the *G* band for SWs and inner tubes of DWs, I_{SW}/I_{DWi}. Taking the experimentally determined purity (80%) by analyzing transmission electron microscopy images and the average value of I_{SW}/I_{DWi} reported in Fig. 5, we find an empirical proportionality factor (633 nm excitation):

$$\frac{N_{SW}}{N_{DW}} \approx 0.3 \frac{I_{SW}}{I_{DWi}}.$$

To understand the proportionality factor of 0.3, we should keep in mind that the spectral *G*-band position for the outer tube is at a higher frequency for DWs than that for SWs (26 and 16 cm^{-1}) and that at atmospheric pressure, the outer tube does not contribute to the *G* band significantly.

We note that considerable reduction in the *G*-band intensity through doping of up to 50% has been reported in the literature,[12] and we observe that the intensity of the *G* band falls exponentially with pressure as $I=I_0 \exp(-0.03\Delta\omega_{outer})$.

IV. PRESSURE MEDIUM- AND TEMPERATURE-INDUCED CHANGES IN THE RAMAN *G* BAND

A. Pressure medium and excitation wavelength

Table I lists the spectral *G*-band positions, pressure coefficients, and relative intensities for the inner and outer tubes and for different pressure media. We find that the pressure medium itself influences the exact spectral position of the *G* band. The larger effect of oxygen on the *G*-band position compared to that of alcohol or argon can be explained by *p* doping of the tubes by oxygen which upshifts the *G* band.[24,25] Chen *et al.*[8] investigated DWs grown from peapods doped with Br_2 (*p* doping) and showed that the charge transfer is dominated by the outer tube with only 10% of the total charge originating from the inner tube.

TABLE II. Parameters for fitting SW/DW spectra in H_2SO_4 (red wavelength excitation).

Wave number (cm^{-1})	HWHM (cm^{-1})
$\omega_{DW\text{-}inner}=1587$	$\Gamma=10$
$\omega_{DW\text{-}outer}=1618$	$\Gamma=10$
$\omega_{SW}=1606$	$\Gamma=10$
$\omega_{DW_{EI}}=1568$	$\Gamma=35$

By fitting the *G* band of DWs, we find a contribution on the lower-frequency side (1560 cm^{-1}), which is also observed for SWs. This band persists with increasing pressure for DWs in contrast with what is observed for SWs.[10] The two *G* bands for both type of DWs (CCVD and peapods) shift at a similar rate with pressure, i.e., 3 and 6 cm^{-1} GPa^{-1} for the inner tubes and the outer ones, when using ethanol-methanol as pressure transmitting medium. In the low-pressure regime (<3 GPa), the two bands overlap and the numerical fit is not stable if the *G* bands of the inner and outer walls are not known. A change in shape can be either due to intensity variation or change in spectral position. We find that there are clear differences between the two types of DWs for the *G* band of the inner tubes when extrapolating from pressure-induced shifts. The spectral position of the inner tube at zero pressure deduced from linear fitting is at 1579 cm^{-1} for the DWs grown from peapods and at 1581 cm^{-1} for DWs grown by CCVD. We also find that the shifting of the *G* band of the inner tube with pressure is delayed for DWs grown by CCVD. This can be explained by differences in the interwall spacing between the two types of DWs with different diameter distributions. This is consistent when deducing the interwall distance in DWs from radial breathing modes . This implies that the coupling of the two walls is not the same, which is consistent with the differences observed for the band at 1560 cm^{-1} attributed to interwall interaction.

When excited at 514 nm as compared to at 633 nm, the spectral position of the *G* band of the inner tube remains the same, while changes in the position of the Fermi level with respect with the excitation energy increases the intensity from the outer tubes (1608 cm^{-1}). In the report of Kim *et al.*,[11] we can see a slight change in the DW *G*-band shape as the signal from the outer tube is reduced, while the signal from the inner tube and the band due to electronic interwall interaction is upshifted (CCVD tubes). *n* doping on DW from peapods show a more complex *G*-band shape.[26] It appears that without doping, the walls are less coupled. *n* doping reduces coupling between the walls due to lattice extension of the outer tube, while *p* doping increases coupling between the walls due to lattice compression of the outer tube.[13]

B. DWs in air and temperature variation

In this section, we use the parameters deduced here and from previous studies[27] on CCVD grown DWs to fit *G*-band spectra as a function of temperature.

TABLE III. Parameters for fitting DW spectra in air (red wavelength excitation).

G band	Electronic contribution
$\Gamma = 10 \times (1 + 0.00146\Delta T)$	$\Gamma_{EI} = 35 \times (1 + 0.003\Delta T)$
$\omega_{inner} = 1581 - 0.024\Delta T$	
$\omega_{outer} = 1592 - 0.024\Delta T$	$\omega_{EI} = 1560 - 0.024\Delta T$

We have previously determined the variation in the half width at half maximum (HWHM) and the spectral *G*-band position with temperature, and we have determined the *G*-band position and the HWHM of DWs in Ar and O_2 at zero pressure using 633 nm excitation.

When excited in the ultraviolet or red spectral region, we find that the HWHMs of the *G* band for the inner and outer tubes range between 8 and 10 cm^{-1}, while the electronic coupling–induced band ranges from 25 to 35 cm^{-1}.

In the absence of any doping, the *G* band of the outer tubes falls in the same spectral range as the *G*+ band of the SWs and we consider only three bands at constant spectral positions and constant HWHM for a given temperature. The parameters used for the three bands including the temperature-induced shifts are listed in Table III.

For the fitting, we use two parameters for the linear background and three parameters for the intensities of the three bands and we include temperature-induced shifts (Table III). Two sets of spectra have been used to test the fitting scheme. The fitted spectra are shown in Fig. 6.

Figure 6 shows the *G* band as a function of laser power using two different microscope objectives and recorded at 633 nm. We find that the fits are only satisfactory when the intensity ratio between inner and outer tube is not kept constant. We find that the intensity associated with the outer tube is small in comparison to the intensity associated with the inner tube as observed before. We notice that at low laser power and without any previous beam exposure, a band appears at 1610 cm^{-1}. As the laser power is increased, the downshift and broadening of all bands is consistent with the increase in temperature as indicated in Table III. At temperatures above 350 °C, the *G* band changes irreversibly, which we attribute to transformation and oxidation of the tubes. This is deduced from the fact that the spectral position is located between 1581 and 1592 cm^{-1} when the laser power is reduced, inconsistent with the temperature-induced spectral shifts.

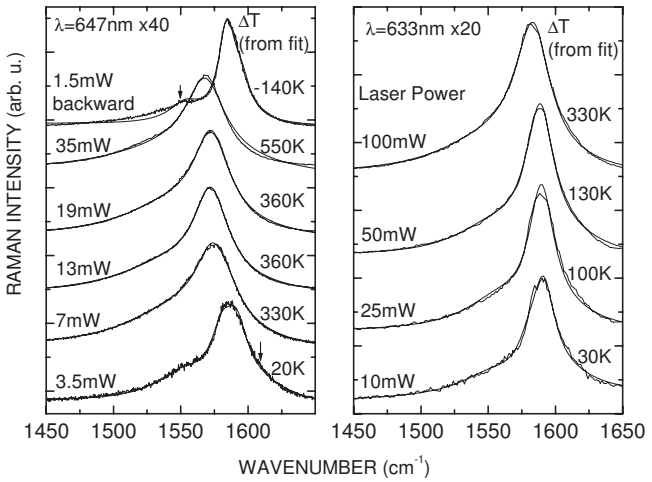

FIG. 6. DW spectra excited with red wavelengths and fitted with the parameters reported in Table III. Arrows indicate that a band at 1550 or 1610 cm^{-1} was used. Laser power and objective power (×40 or ×20) are also indicated.

V. CONCLUSION

We find that chemical doping with H_2SO_4 and using hydrostatic pressure, we can extrapolate the *G*-band position of the inner and outer tubes. The fitted spectral intensity, assuming fixed spectral positions for contributions from inner and outer walls of DWs and SWs, is used to determine the purity of CCVD DWs containing SWs. Apart from the contributions of the *G* band of the inner and outer tubes at 1581 and 1592 cm^{-1}, a band related to electronic interwall interaction at 1560 cm^{-1} is observed. This band is associated with the outer tubes due to the fact that it shifts with pressure at the same rate as the outer tubes. When chemical doping with H_2SO_4 is considered, this additional band persists, contrary to what is observed for SWs, where the band disappears when doping. *G* bands from DWs recorded in air and at different temperatures can be explained by using constant *G*-band positions for inner and outer walls.

ACKNOWLEDGMENT

We thank Jenny Patterson, Intel Ireland, for stimulating discussions.

*pascal.puech@cemes.fr

[1] K. Matsubara, K. Sugihara, and T. Tsuzuku, Phys. Rev. B **41**, 969 (1990).

[2] B. Bourlon, C. Miko, L. Forro, D. C. Glattli, and A. Bachtold, Phys. Rev. Lett. **93**, 176806 (2004).

[3] S. Bandow, M. Takizawa, K. Hirahara, M. Yudasaka, and S. Iijima, Chem. Phys. Lett. **337**, 48 (2001).

[4] E. Flahaut, A. Peigney, Ch. Laurent, and A. Rousset, J. Mater. Chem. **10**, 249 (2000).

[5] M. Endo, H. Muramatsu, T. Hayashi, Y. A. Kim, M. Terrones, and M. S. Dresselhaus, Nature (London) **433**, 476 (2005).

[6] C. Thomsen and S. Reich, in *Light Scattering in Solids IX*, edited by M. Cardona and R. Merlin (Springer-Verlag, Berlin Heidelberg, 2005).

[7] Ladislav Kavan and Lothar Dunsch, ChemPhysChem **8**, 974 (2007).

[8] G. Chen, S. Bandow, E. R. Margine, C. Nisoli, A. N. Kolmogorov, V. H. Crespi, R. Gupta, G. U. Sumanasekera, S. Iijima, and P. C. Eklund, Phys. Rev. Lett. **90**, 257403 (2003).

[9] P. Puech, E. Flahaut, A. Sapelkin, H. Hubel, D. J. Dunstan, G.

Landa, and W. S. Bacsa, Phys. Rev. B **73**, 233408 (2006).
[10] A. Merlen, N. Bendiab, P. Toulemonde, A. Aouizerat, A. San Miguel, J. L. Sauvajol, G. Montagnac, H. Cardon, and P. Petit, Phys. Rev. B **72**, 035409 (2005).
[11] Y. A. Kim, H. Muramatsu, M. Kojima, T. Hayashi, M. Endo, M. Terrones, and M. S. Dresselhaus, Chem. Phys. Lett. **420**, 377 (2006).
[12] W. Zhou, J. Vavro, N. M. Nemes, J. E. Fischer, F. Borondics, K. Kamaras, and D. B. Tanner, Phys. Rev. B **71**, 205423 (2005).
[13] E. B. Barros, H. Son, Ge. G. Samsonidze, A. G. Souza Filho, R. Saito, Y. A. Kim, H. Muramatsu, T. Hayashi, M. Endo, J. Kong, and M. S. Dresselhaus, Phys. Rev. B **76**, 045425 (2007).
[14] P. Puech, H. Hubel, D. J. Dunstan, R. R. Bacsa, C. Laurent, and W. S. Bacsa, Phys. Rev. Lett. **93**, 095506 (2004).
[15] J. Arvanitidis, D. Christofilos, K. Papagelis, K. S. Andrikopoulos, T. Takenobu, Y. Iwasa, H. Kataura, S. Ves, and G. A. Kourouklis, Phys. Rev. B **71**, 125404 (2005).
[16] E. Flahaut, R. Bacsa, A. Peigney, and Ch. Laurent, Chem. Commun. (Cambridge) **2003**, 1442.
[17] A. Bassil, P. Puech, L. Tubery, W. Bacsa, and E. Flahaut, Appl. Phys. Lett. **88**, 173113 (2006).
[18] C. T. Chan, W. A. Kamitakahara, K. M. Ho, and P. C. Eklund, Phys. Rev. Lett. **58**, 1528 (1987).
[19] R. Nishitani, Y. Sasaki, and Y. Nishina, Phys. Rev. B **37**, 3141 (1988).
[20] M. Hanfland, H. Beister, and K. Syassen, Phys. Rev. B **39**, 12598 (1989).
[21] S. Piscanec, M. Lazzeri, J. Robertson, A. C. Ferrari, and F. Mauri, Phys. Rev. B **75**, 035427 (2007).
[22] W. Zhou, J. E. Fischer, P. A. Heiney, H. Fan, V. A. Davis, M. Pasquali, and R. E. Smalley, Phys. Rev. B **72**, 045440 (2005).
[23] D. S. Kim and P. Y. Yu, Phys. Rev. B **43**, 4158 (1991).
[24] P. Corio, A. P. Santos, P. S. Santos, M. L. A. Temperini, V. W. Brar, M. A. Pimenta, and M. S. Dresselhaus, Chem. Phys. Lett. **383**, 475 (2004).
[25] S. B. Fagan, A. G. Souzafilho, J. Mendes Filho, P. Corio, and M. S. Dresselhaus, Chem. Phys. Lett. **406**, 54 (2005).
[26] H. Rauf, T. Pichler, R. Pfeiffer, F. Simon, H. Kuzmany, and V. N. Popov, Phys. Rev. B **74**, 235419 (2006).
[27] P. Puech, F. Puccianti, R. Bacsa, C. Arrondo, V. Paillard, A. Bassil, M. Monthioux, E. Flahaut, F. Bardé, and W. Bacsa, Phys. Rev. B **76**, 054118 (2007).